



Error identification entanglement purification for stationary system using high-dimensional entanglement

Ji Qi,¹ Ke Li,¹ Zhe Yang ,^{1,2} Rui-Yang Yuan,¹ and Bao-Cang Ren ^{1,*}

¹*Department of Physics, Capital Normal University, Beijing 100048, China*

²*Key Laboratory of Terahertz Optoelectronics (MoE), Capital Normal University, Beijing 100048, China*



(Received 14 November 2023; accepted 2 April 2024; published 23 April 2024)

High-fidelity entanglement plays an important role in quantum networks for guaranteeing the integrity of quantum information processing. We present an error identification entanglement purification protocol (EIEPP) for maintaining high-fidelity entanglement of stationary systems. In EIEPP, the hybrid controlled- x gate for stationary systems and high-dimensional spatial-mode state of photons has been constructed using a stationary-whispering gallery mode resonator-waveguides system, and it is used to construct an error number gate (ENG) and error position gate (EPG) for noisy entangled stationary systems. Using ENG and EPG, the stationary systems with errors are discarded according to the measurement results of high-dimensional entangled photon states, and typically high-fidelity entangled states of stationary systems can be achieved with high yield in both ideal and practical situations. This EIEPP has superior performance for stationary systems with amplitude damping noise, and it is also applicable for stationary systems with other types of noise.

DOI: [10.1103/PhysRevA.109.042423](https://doi.org/10.1103/PhysRevA.109.042423)

I. INTRODUCTION

Entanglement is a vital resource for numerous applications in quantum information protocols and technologies, such as quantum networks [1,2], quantum communication [3–15], quantum repeaters [16–20], distributed quantum computation [21,22], and so on. Nonetheless, entanglement is fragile under noise and decoherence in the distribution and storage processes, which may influence the performance of quantum information protocols and technologies. Entanglement purification [23] is a passive way for maintaining high-fidelity entanglement, where fewer copies of the entangled state with increased fidelity are produced by locally manipulating ensembles of noisy entangled states.

In the past decades, many entanglement purification protocols (EPPs) have been proposed and demonstrated using several methods [23–53], such as recurrence protocols, hashing protocols, breeding protocols, and so on. Recurrence EPPs [23–26] involve the controlled-NOT gate operations (or similar operations) and measurements on few copies of noisy entangled states, and these protocols are always iteratively applied to increase the fidelity of the entangled state probabilistically. Hashing and breeding protocols [23–25] require operations on (asymptotically) large ensembles and extra entanglement to gather the information of errors in noisy ensemble by measuring parities of randomly chosen subsets. Nevertheless, the asymptotic schemes may repeatedly access and interpret partial information and exclude many incompatible state configurations.

In the practical application, it is important to design entanglement purification protocols with both high yields and high error thresholds, which is a bottleneck to be overcome. In

2021, Riera-Sàbat *et al.* introduced an entanglement purification scheme named error identification protocol (EIP) [54,55] using the high-dimensional entangled states as auxiliary. In EIP, the number and position information of errors in an ensemble of noisy entangled states can be transferred to the high-dimensional entangled states, resulting in the purification of the ensemble. This approach offers an efficient and direct way to perform entanglement purification on systems involving a limited number of copies. Moreover, EIP may lead to a perfect entangled state with unit fidelity in a deterministic manner, if the number of errors in the ensemble is bounded and the local operations are perfect. If there are too many errors in the ensemble, EIP may work in a probabilistic manner to avoid the cost of more entanglement than can be gained, while the achievable fidelity of this manner could also be typically high with an improved yield in some cases.

Quantum stationary systems [48,56] are artificial solid atom systems that are more stable than photonic systems, and they are natural candidates for quantum networking applications. The negatively charged silicon-vacancy color (SiV^-) center in diamond is a fantastic stationary system [57–59] which has attracted much attention with high brightness [60], lifetime-limited optical linewidths [61], and narrow inhomogeneous distribution of optical transition frequencies [62]. The unique inversion symmetry of the SiV^- center causes the permanent electric dipole moments of the ground and excited states to disappear, making the transition insensitive to the electric field noise typically present in nanostructures [63]. This property makes the SiV^- center a promising candidate for solid-state qubit of a quantum network node [56], especially in cavity quantum electrodynamics (QED). Moreover, the entanglement of SiV^- centers can be created by using a portion of the coherent photons emitted in the zero phonon line (ZPL) [64].

*Corresponding author: renbaocang@cnu.edu.cn

Here, we present an error identification entanglement purification protocol (EIEPP) for the SiV^- center system, which can achieve typically high fidelity and high yield in both ideal and practical situations. Error number gate (ENG) and error position gate (EPG) are two essential elements of this EIEPP, and they are constructed by the hybrid controlled-X (CX) gate of SiV^- center in diamond and the four-dimensional spatial-mode state of a photon. Using ENG and EPG, the number and position information of errors in an ensemble of noisy entangled SiV^- center systems will be transferred to four-dimensional photonic Bell states, and the SiV^- center systems with errors could be discarded according to the measurement results of four-dimensional photon states, resulting in high-fidelity entangled states of SiV^- center systems. For the SiV^- center systems with amplitude damping noise, the purified state in EIEPP has nearly unit fidelity with perfect local operations. Additionally, the EIEPP for SiV^- center systems suffering from other types of noise has also been analyzed briefly. Furthermore, the fidelity of the purified state and the yield of EIEPP are discussed in an experimental situation, which shows that EIEPP can achieve comparable average fidelity and high yield even with imperfect local operations. Therefore, this EIEPP has promising applications in practical quantum information protocols and technologies.

The paper is organized as follows. In Sec. II, we introduce the construction and application of a hybrid CX gate for the SiV^- center system and four-dimensional spatial-mode state of a photon. In Sec. III, we introduce the construction of ENG and EPG and the implementation of EIEPP. In Sec. IV, we discuss the feasibility of EIEPP in an experimental situation. Finally, we present a conclusion in Sec. V.

II. HYBRID CONTROLLED-X GATE

A. Construction of hybrid controlled-x gate

In this section, we will construct a hybrid CX gate for the quantum state of a SiV^- center in diamond and the four-dimensional spatial-mode state of a photon. The SiV^- center in diamond has been identified as a promising stationary qubit for carrying information due to its unique structure, which consists of complexes made up of two carbon vacancies with a silicon atom between them [56–59], as shown in Fig. 1(a). The unique structure of the SiV^- center exhibits D_{3d} inversion symmetry [58]. Under the moderate strain, the ground state of the SiV^- center can be simplified to the two electron-spin sublevels of the lowest orbital branch, i.e., $|g\rangle = |\downarrow\rangle$ and $|e\rangle = |\uparrow\rangle$, and the excited state of the SiV^- center can also be simplified to two electron-spin levels of the lower orbital branch, i.e., $|g'\rangle = |\downarrow\rangle$ and $|e'\rangle = |\uparrow\rangle$ [56,58], as shown in Fig. 1(b). This simplification can be achieved by removing uncorrelated energy levels of the SiV^- center with large detunings. When an external magnetic field is applied along the SiV^- symmetry axis, the spin-conserving optical transitions $|g\rangle \leftrightarrow |g'\rangle$ and $|e\rangle \leftrightarrow |e'\rangle$ will occur independently with horizontal polarization photons ($|H\rangle$) in the frequencies ω_g and $\omega_e = \omega_g + \Delta$, respectively, while the cross transitions $|g\rangle \leftrightarrow |e'\rangle$ and $|e\rangle \leftrightarrow |g'\rangle$ with spin flipping are dipole forbidden [56,58].

The transitions between $|g\rangle \leftrightarrow |g'\rangle$ and $|e\rangle \leftrightarrow |e'\rangle$ can be enhanced by fixing the SiV^- center on the exterior surface

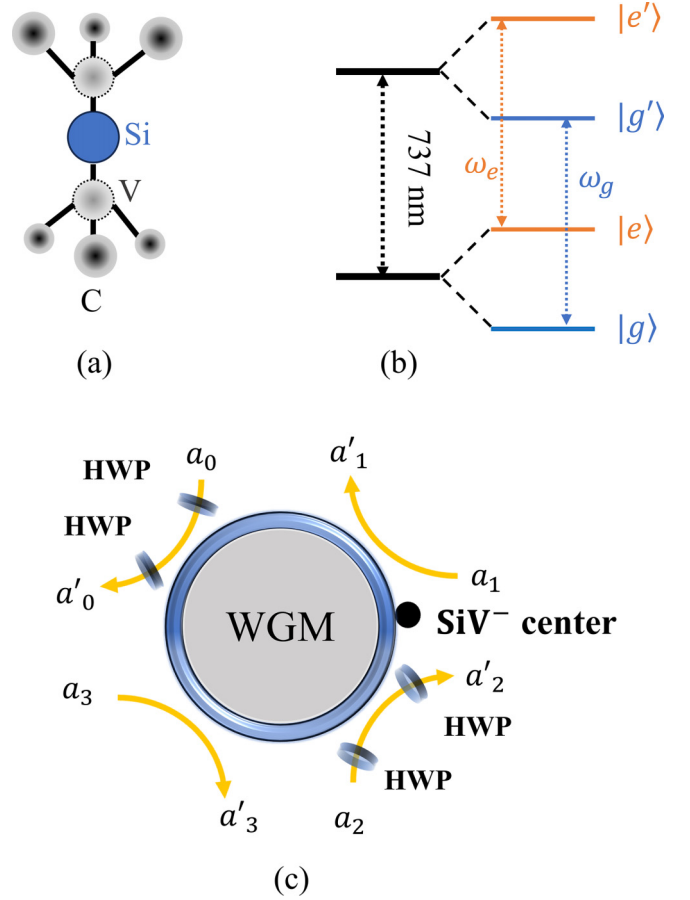


FIG. 1. (a) Atomic structure of SiV^- center in diamond. (b) The energy-level structure of SiV^- center and its optical transition. $|g\rangle$ and $|e\rangle$ represent two electron-spin sublevels of the lowest orbital branch in the ground state. $|g'\rangle$ and $|e'\rangle$ represent two electron-spin levels of the lower orbital branch in the excited state [56]. (c) Schematic diagram of a hybrid controlled-X gate constructed by SiV^- -WGM-waveguides-HWP system. $a_0 - a_3$ ($a'_0 - a'_3$) are input (output) ports of four waveguides coupled to WGM resonator. HWP represents the half-wave plate with function $|H\rangle \rightarrow -|H\rangle$ and $|V\rangle \rightarrow |V\rangle$.

of a whispering gallery mode (WGM) resonator [65–68] as shown in Fig. 1(c). Here, $a_0 - a_3$ ($a'_0 - a'_3$) are input (output) ports of four waveguides coupled to a WGM resonator. In this SiV^- -WGM-waveguides system, the interaction of the input photon and SiV^- center can be deduced by the quantum Heisenberg equation of motion for the cavity-mode operator \hat{a} and the dipole operator $\hat{\sigma}_-$ in the interaction picture [68–70]. That is,

$$\begin{aligned} \frac{d\hat{a}}{dt} &= -i(\omega_c - \omega_p)\hat{a} - \frac{\kappa_1 + \kappa_2}{2}\hat{a} - g\hat{\sigma}_- \\ &\quad + \sqrt{\kappa_1}\hat{a}_j + \sqrt{\kappa_2}\hat{a}_{j\oplus 1}, \\ \frac{d\hat{\sigma}_-}{dt} &= -\left[i(\omega_s - \omega_p) + \frac{\gamma}{2}\right]\hat{\sigma}_- - g\hat{\sigma}_z\hat{a}, \end{aligned} \quad (1)$$

where ω_c represents the frequency of the resonator field. ω_p represents the frequency of the input photon, and ω_s represents the frequency of the dipole transition ($s = g, e$). $\hat{\sigma}_-$ and $\hat{\sigma}_z$ represent the lowering operator and the inversion operator of the

SiV⁻ center. γ stands for the spontaneous emission rate of the SiV⁻ center, and g is the coupling strength between the WGM resonator and the SiV⁻ center. The operators \hat{a}_j ($\hat{a}_{j\ominus 1}$) and \hat{a}'_j ($\hat{a}'_{j\ominus 1}$) are the input and output field operators, respectively, where $j = 0, 1, 2, 3$ and $j \ominus 1 = (j - 1) \bmod 4$. They satisfy the boundary relations $\hat{a}'_j = \hat{a}_j - \sqrt{\kappa_1}\hat{a}$ and $\hat{a}'_{j\ominus 1} = \hat{a}_{j\ominus 1} - \sqrt{\kappa_2}\hat{a}$. κ_1 and κ_2 represent the coupling losses of WGM-bus and WGM-drop waveguides, respectively, and $\kappa_1 = \kappa_2$ can be adjusted to ensure maximum coupling efficiency [65].

In the weak excitation limit with the SiV⁻ center dominant in the ground state ($\langle \sigma_z \rangle = -1$), the steady-state solution of transmittance and reflectance of the SiV⁻-WGM-waveguides system can be obtained [68]. The reflection coefficient [$r(\omega_p)$] and transmission coefficient [$t(\omega_p)$] can be expressed as

$$\begin{aligned} t(\omega_p) &= \frac{i(\omega_c - \omega_p)[i(\omega_s - \omega_p) + \frac{\gamma}{2}] + g^2}{[i(\omega_c - \omega_p) + \kappa][i(\omega_s - \omega_p) + \frac{\gamma}{2}] + g^2}, \\ r(\omega_p) &= \frac{-\kappa[i(\omega_s - \omega_p) + \frac{\gamma}{2}]}{[i(\omega_c - \omega_p) + \kappa][i(\omega_s - \omega_p) + \frac{\gamma}{2}] + g^2}. \end{aligned} \quad (2)$$

At resonance condition with $\omega_c = \omega_p$, the transmission and reflection coefficients of the SiV⁻-WGM-waveguides system can be written as

$$\begin{aligned} t(\omega_p) &= \frac{g^2}{\kappa[i(\omega_s - \omega_p) + \frac{\gamma}{2}] + g^2}, \\ r(\omega_p) &= \frac{-\kappa[i(\omega_s - \omega_p) + \frac{\gamma}{2}]}{\kappa[i(\omega_s - \omega_p) + \frac{\gamma}{2}] + g^2}. \end{aligned} \quad (3)$$

The input photon is in the $|H\rangle$ state with $\omega_p \approx \omega_g$. For the case $\omega_s = \omega_e$, the SiV⁻ center is uncoupled to the WGM resonator ($g = 0$), with the input photon resonant with the bare WGM resonator, and the transmission and reflection coefficients are $t_0 = 0$ and $r_0 = -1$ with phase shift $\phi_0 = \pi$. On the other hand, under the resonance condition ($\omega_s = \omega_g$), the transmission and reflection coefficients can be expressed as

$$t = \frac{2g^2}{\gamma\kappa + 2g^2}, \quad r = \frac{-\gamma\kappa}{\gamma\kappa + 2g^2}. \quad (4)$$

When the SiV⁻ center is strongly coupled to the resonator ($g \gg \sqrt{\gamma\kappa}$), the reflection and transmission coefficients are $r \rightarrow 0$ and $t \rightarrow 1$ with no phase shift ($\phi = 0$). Then, the input-output rule of the input photon interacting with the SiV⁻-WGM-waveguides system can be summarized as

$$|a_j, g\rangle \rightarrow |a'_j, g\rangle, \quad |a_j, e\rangle \rightarrow -|a'_{j\ominus 1}, e\rangle. \quad (5)$$

In Eq. (5), if the state of the SiV⁻ center is $|g\rangle$, the photon is input and output from the same waveguide (the subscript of the output port is the same as the subscript of the input port), which corresponds to the case where the spatial-mode state of the photon remains unchanged. If the state of the SiV⁻ center is $|e\rangle$, the photon is input from a waveguide j and output from the adjacent waveguide $j \ominus 1$ [69], which corresponds to the case where the spatial-mode state of the photon will be flipped from $|a_j\rangle$ to $|a'_{j\ominus 1}\rangle$ with an additional π phase shift. Here, the additional π phase shift can be eliminated by the half-wave plates (HWPs) shown in Fig. 1(c), whose function can be expressed as $|H\rangle \rightarrow -|H\rangle$ and $|V\rangle \rightarrow |V\rangle$. Hence,

the input-output rule of the input photon interacting with the SiV⁻-WGM-waveguides-HWP system can be expressed as

$$|a_j, g\rangle \rightarrow |a'_j, g\rangle, \quad |a_j, e\rangle \rightarrow |a'_{j\ominus 1}, e\rangle. \quad (6)$$

Equation (6) is the function of the hybrid CX gate, where the control qubit is the state of the SiV⁻ center and the target qudit is the spatial-mode state (i.e., four waveguides) of the input photon. That is, if the state of the SiV⁻ center is $|g\rangle$, the spatial-mode state of the photon remains unchanged. If the state of the SiV⁻ center is $|e\rangle$, the spatial-mode state of the photon is flipped from $|a_j\rangle$ to $|a'_{j\ominus 1}\rangle$.

B. The application of hybrid CX gate

In this section, we will investigate the function of hybrid CX gates for the Bell states of the SiV⁻ center system and four-dimensional photon system. The four Bell states of the SiV⁻ center system can be expressed as

$$\begin{aligned} |\phi^+\rangle_{\text{Si}_1\text{Si}_2} &= \frac{1}{\sqrt{2}}(|gg\rangle + |ee\rangle)_{\text{Si}_1\text{Si}_2}, \\ |\psi^+\rangle_{\text{Si}_1\text{Si}_2} &= \frac{1}{\sqrt{2}}(|ge\rangle + |eg\rangle)_{\text{Si}_1\text{Si}_2}, \\ |\phi^-\rangle_{\text{Si}_1\text{Si}_2} &= \frac{1}{\sqrt{2}}(|gg\rangle - |ee\rangle)_{\text{Si}_1\text{Si}_2}, \\ |\psi^-\rangle_{\text{Si}_1\text{Si}_2} &= \frac{1}{\sqrt{2}}(|ge\rangle - |eg\rangle)_{\text{Si}_1\text{Si}_2}, \end{aligned} \quad (7)$$

where Si_1 (Si_2) represents the SiV⁻ center in the SiV⁻₁-WGM₁-waveguides-HWP (SiV⁻₂-WGM₂-waveguides-HWP) system. The Bell state of the four-dimensional photon system is expressed as [55]

$$|\Psi_{mn}\rangle = \frac{1}{2} \sum_{k=0}^3 e^{i\frac{\pi}{2}km} |a_k\rangle_A |b_{k\ominus n}\rangle_B, \quad (8)$$

where A and B represent two photons of four-dimensional Bell states. The subindex m is defined as the phase index, and the subindex n is defined as the amplitude index ($m, n = 0, 1, 2, 3$). $|a_k\rangle_A$ and $|b_{k\ominus n}\rangle_B$ represent the spatial modes of photons A and B , respectively, and they correspond to the input ports of two SiV⁻-WGM-waveguides-HWP systems shown in Fig. 2. The polarization modes of photons A and B are both in $|H\rangle$ state.

Two hybrid CX gates are performed on the Bell states of two SiV⁻ centers and two photons. That is, the states of Si_1 and Si_2 are used as the control qubits of the first hybrid CX gate and second hybrid CX gate, respectively, and spatial-mode states of two photons A and B are used as the target qudits of the first hybrid CX gate and second hybrid CX gate, respectively. After the two hybrid CX gates performed on the Bell states of two SiV⁻ centers and two photons, the quantum state of system Si_1Si_2AB will be transformed to

$$\begin{aligned} |\phi^+\rangle_{\text{Si}_1\text{Si}_2} |\Psi_{00}\rangle_{AB} &\mapsto |\phi^+\rangle_{\text{Si}_1\text{Si}_2} |\Psi'_{00}\rangle_{AB}, \\ |\phi^-\rangle_{\text{Si}_1\text{Si}_2} |\Psi_{00}\rangle_{AB} &\mapsto |\phi^-\rangle_{\text{Si}_1\text{Si}_2} |\Psi'_{00}\rangle_{AB}, \\ |eg\rangle_{\text{Si}_1\text{Si}_2} |\Psi_{00}\rangle_{AB} &\mapsto |eg\rangle_{\text{Si}_1\text{Si}_2} |\Psi'_{03}\rangle_{AB}, \\ |ge\rangle_{\text{Si}_1\text{Si}_2} |\Psi_{00}\rangle_{AB} &\mapsto |ge\rangle_{\text{Si}_1\text{Si}_2} |\Psi'_{01}\rangle_{AB}. \end{aligned} \quad (9)$$

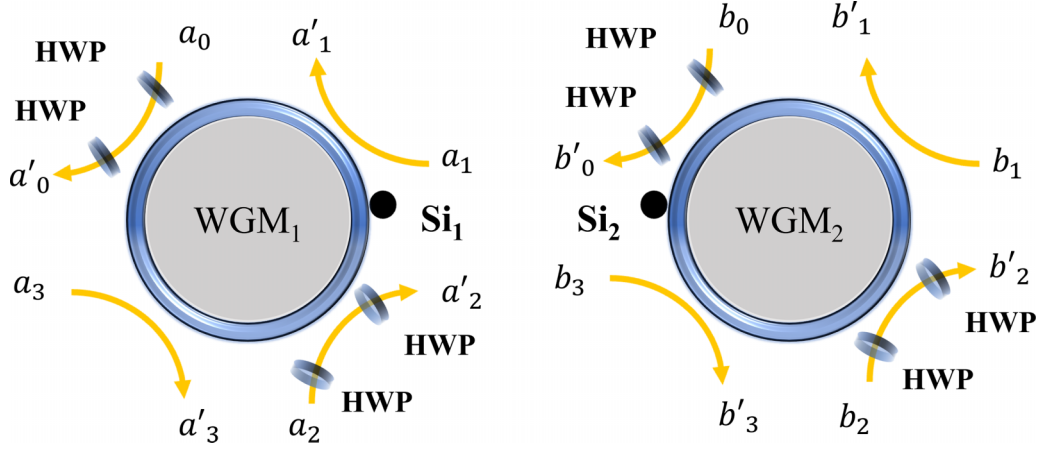


FIG. 2. Schematic diagram of hybrid CX gates for the Bell states of the SiV^- center system and four-dimensional photon system. Photon A and SiV^- center system Si_1 belong to Alice. Photon B and SiV^- center system Si_2 belong to Bob. $a_0 - a_3$ ($a'_0 - a'_3$) are input (output) ports of the SiV_1^- -WGM₁-waveguides-HWP system. $b_0 - b_3$ ($b'_0 - b'_3$) are input (output) ports of the SiV_2^- -WGM₂-waveguides-HWP system.

Here,

$$|\Psi'_{mn}\rangle = \frac{1}{2} \sum_{k=0}^3 e^{i\frac{\pi}{2}km} |a'_k\rangle_A |b'_{k\oplus n}\rangle_B. \quad (10)$$

$|a'_k\rangle_A$ and $|b'_{k\oplus n}\rangle_B$ represent the spatial modes of photons A and B , which correspond to the output ports of two SiV^- -WGM-waveguides-HWP systems shown in Fig. 2.

From Eq. (9), we can find that the parity information of Bell states of Si_1Si_2 can be identified by the four-dimensional photonic Bell state. If the state of Si_1Si_2 is $|ge\rangle$ (odd parity), the amplitude index of the four-dimensional photonic Bell state is increased by one (i.e., $n = 0 \rightarrow n = 1$). Besides, if the state of Si_1Si_2 is $|eg\rangle$ (odd parity), the amplitude index of the four-dimensional photonic Bell state is decreased by one (i.e., $n = 0 \rightarrow n = 3$). For the Bell states $|\phi^+\rangle_{\text{Si}_1\text{Si}_2}$ and $|\phi^-\rangle_{\text{Si}_1\text{Si}_2}$ (even parity), the amplitude index of the four-dimensional photonic Bell state remains unchanged. By measuring the spatial-mode states of photons A and B , the variation of amplitude index of the four-dimensional photonic Bell state can be read out, which means the parity information of the quantum state of Si_1Si_2 can be identified. In Sec. III, we will use this function of hybrid CX gates to construct the EIEPP.

III. ERROR IDENTIFICATION ENTANGLEMENT PURIFICATION PROTOCOL

In quantum information processing, SiV^- center systems in the maximally entangled Bell state will decay to the ones in the less-entangled mixed state by the environment noise. For example, SiV^- center systems in Bell state $|\phi^+\rangle$ will decay to the ones in less-entangled mixed state ρ by several particular types of noise, such as amplitude damping noise, dephasing noise, or bit-flip noise. Here, the less-entangled mixed state can be described as

$$\rho = p_0|\phi^+\rangle\langle\phi^+| + p_1|ge\rangle\langle ge| + p_2|eg\rangle\langle eg|. \quad (11)$$

The fidelity of the Bell state $|\phi^+\rangle$ in mixed state ρ is $F = p_0$, and the probabilities of the error components $|ge\rangle$ and $|eg\rangle$ in

mixed state ρ are p_1 and p_2 , respectively, where $p_0 + p_1 + p_2 = 1$.

Here, we will introduce an EIEPP to reduce the probabilities of the error components in mixed state ρ , which means the fidelity of the Bell state $|\phi^+\rangle$ in mixed state ρ can be increased. In order to implement EIEPP, the nonlocal mixed entangled SiV^- center systems are divided into several subsets, and each subset contains four nonlocal mixed entangled SiV^- center systems (i.e., $\text{Si}_1^1\text{Si}_2^1 - \text{Si}_1^4\text{Si}_2^4$) as shown in Fig. 3, where $\text{Si}_1^1 - \text{Si}_1^4$ belong to Alice and $\text{Si}_2^1 - \text{Si}_2^4$ belong to Bob. The remote users first identify the number of error SiV^- center systems in each subset using ENG, and then they identify the position of error SiV^- center systems in each subset using EPG. At last, the error components in mixed state ρ can be

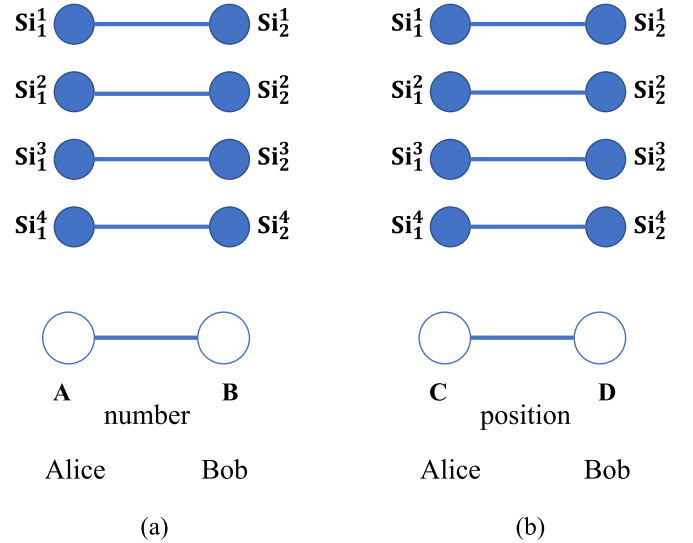


FIG. 3. Schematic diagram of error identification entanglement purification protocol. (a) Error number gate. (b) Error position gate. $\text{Si}_1^1\text{Si}_2^1 - \text{Si}_1^4\text{Si}_2^4$ represent four SiV^- center systems in a subset. SiV^- centers $\text{Si}_1^1 - \text{Si}_1^4$ and photons AC belong to Alice. SiV^- centers $\text{Si}_2^1 - \text{Si}_2^4$ and photons BD belong to Bob. The schematic diagrams of ENG and EPG are shown in Fig. 4.

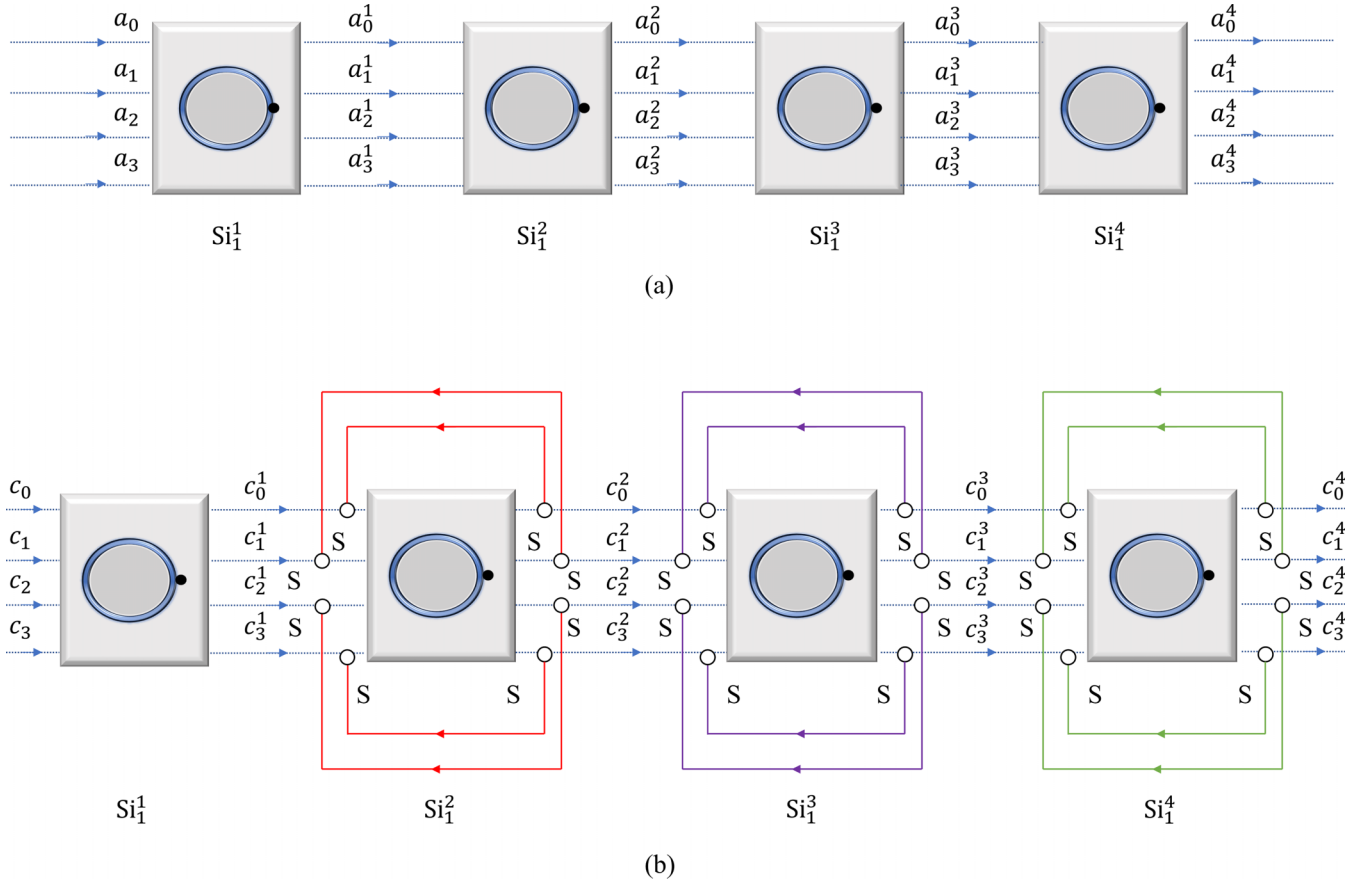


FIG. 4. Schematic diagrams of (a) ENG and (b) EPG in Alice's side. S represents an optical switch [71], and it is used to convey photon C from the output port $c_k^{y\oplus 1}$ to the corresponding input port c_k^y ($y = 1, 2, 3$). The schematic diagrams of ENG and EPG in Bob's side are similar to the ones in Alice's side by replacing Si_1^y and photons AC to Si_2^y and photons BD .

removed according to the number and position information of error SiV^- center systems in each subset, resulting in high-fidelity entangled states of SiV^- center systems.

A. Error number gate and error position gate

In EIEPP, ENG and EPG are used to identify the number and position of error SiV^- center systems in each subset, and they are constructed by the hybrid CX gate introduced in Sec. II. The quantum circuits of ENG and EPG are shown in Figs. 4(a) and 4(b), respectively.

In ENG, an auxiliary four-dimensional photonic Bell state $|\Psi_{00}\rangle_{AB}$ is required, where two photons A and B belong to the remote users Alice and Bob, respectively. The remote user Alice (Bob) performs hybrid CX gates on photon A (B) and four SiV^- centers $\text{Si}_1^1 - \text{Si}_1^4$ ($\text{Si}_2^1 - \text{Si}_2^4$) in sequence as shown in Fig. 4(a). Here, the superscript y ($y = 1, 2, 3, 4$) represents the position of the SiV^- center in the subset. The explicit expression of ENG is given by [55]

$$\prod_{y=1}^4 \text{CX}_{\text{Si}_1^y \rightarrow A} \text{CX}_{\text{Si}_2^y \rightarrow B}, \quad (12)$$

where the subscript $\text{Si}_1^y \rightarrow A$ ($\text{Si}_2^y \rightarrow B$) represents that the control qubit of the hybrid CX gate is the state of Si_1^y (Si_2^y) and the target qubit of the hybrid CX gate is the spatial-mode state

of photon A (B). Then, Alice and Bob measure the spatial-mode states of two photons A and B , and they compare their measurement results. If the measurement results show that the spatial-mode states of two photons A and B are $|a'_k\rangle_A$ and $|b'_{k \oplus n}\rangle_B$, the number of error SiV^- center systems $|ge\rangle$ (or $|eg\rangle$) in a subset can be identified by the relationship $n = n_e \bmod 4$ [or $n = (4 - n_e) \bmod 4$], where n_e represents the number of error SiV^- center systems in a subset.

In EPG, another auxiliary four-dimensional photonic Bell state $|\Psi_{00}\rangle_{CD}$ is required, where two photons C and D belong to the remote users Alice and Bob, respectively. The remote user Alice (Bob) performs hybrid CX gates on photon C (D) and four SiV^- centers $\text{Si}_1^1 - \text{Si}_1^4$ ($\text{Si}_2^1 - \text{Si}_2^4$) in sequence as shown in Fig. 4(b). Here, the hybrid CX gate for Si_1^y (Si_2^y) will be performed y times. That is, the hybrid CX gate for photon C (D) and SiV^- center Si_1^1 (Si_2^1) is performed once. Then, the hybrid CX gate for photon C (D) and SiV^- center Si_1^2 (Si_2^2) is performed twice. Subsequently, the hybrid CX gate for photon C (D) and SiV^- center Si_1^3 (Si_2^3) is performed three times. Finally, the hybrid CX gate for photon C (D) and SiV^- center Si_1^4 (Si_2^4) is performed four times. The explicit expression of the EPG is given by [55]

$$\prod_{y=1}^4 (\text{CX}_{\text{Si}_1^y \rightarrow C})^y (\text{CX}_{\text{Si}_2^y \rightarrow D})^y. \quad (13)$$

TABLE I. The relationship of n , n_e , configuration, additional operations, and fidelity of purified state for the case $p_2 = 0$.

n	n_e	Configuration	Additional operation	F'
0	0 or 4	$4 \times \phi^+\rangle$ or $4 \times ge\rangle$	/	$\frac{F^4}{F^4+(1-F)^4}$
1	1	$1 \times ge\rangle$	EPG	1
2	2	$2 \times ge\rangle$	Grouping	1
3	3	$3 \times ge\rangle$	EPG	1

Then, Alice and Bob measure the spatial-mode states of two photons C and D , and they compare their measurement results. If the measurement results show that the spatial-mode states of two photons C and D are $|c'_k\rangle_C$ and $|d'_{k \oplus n'}\rangle_D$, the position y_e of error SiV⁻ center system $|ge\rangle$ (or $|eg\rangle$) in a subset can be identified by the relationship $n' = (\sum_{y_e=1}^{y_e=n_e} y_e) \bmod 4$ (or $n' = [4 - (\sum_{y_e=1}^{y_e=n_e} y_e)] \bmod 4$).

B. Error identification entanglement purification protocol

Here, we introduce the way to purify the less-entangled mixed state ρ using ENG and EPG (i.e., the detailed procedure of EIEPP). For the sake of simplification, we first introduce the detailed procedures of EIEPP for the cases $p_2 = 0$ and $p_1 = 0$ in Eq. (11). Subsequently, we discuss the EIEPP procedures for the cases $p_2 = p_1$ and $p_2 \neq p_1 \neq 0$ in Eq. (11).

1. $p_2=0$

In this case, the quantum state of the SiV⁻ center system in Eq. (11) can be expressed as

$$\rho_1 = F|\phi^+\rangle\langle\phi^+| + (1-F)|ge\rangle\langle ge|, \quad (14)$$

which is local unitary (LU) equivalent to the result of sending a Bell state through an amplitude damping channel [54,55,72]. Alice and Bob perform the ENG operation on four SiV⁻ center systems $\text{Si}_1^1\text{Si}_2^1 - \text{Si}_1^4\text{Si}_2^4$ in a subset using four-dimensional photonic Bell state $|\Psi_{00}\rangle_{AB}$. Then, Alice and Bob measure the spatial-mode states of two photons A and B , and they can read out the number (n_e) of error SiV⁻ center systems (i.e., $|ge\rangle\langle ge|$) in this subset using the relationship $n = n_e \bmod 4$. Subsequently, Alice and Bob have to perform different operations for the four conditions obtained by the amplitude index n of this ENG operation. The relationships of n , n_e , configuration, additional operations, and fidelity of purified state are shown in Table I.

a. $n = 0$. In this condition, the number of error SiV⁻ center systems in this subset could be $n_e = 0$ (or $n_e = 4$), which corresponds to the configuration where four SiV⁻ center systems $\text{Si}_1^1\text{Si}_2^1 - \text{Si}_1^4\text{Si}_2^4$ are in state $|\phi^+\rangle$ (or $|ge\rangle$). The probability of the case $n_e = 4$ is much smaller than the one of $n_e = 0$. For example, the probability of $n_e = 4$ is only 0.16% when $F = 0.8$, which is much smaller than the one of $n_e = 0$ with 40.96%. Therefore, the result $n = 0$ of this ENG is deemed to be the successful condition of EIEPP, and the EPG operation is not required in this condition. The fidelity of the purified state of this condition is shown in Table I.

b. $n = 1$. In this condition, the number of error SiV⁻ center systems in this subset is $n_e = 1$, which corresponds to the

configuration where one SiV⁻ center system in this subset is in state $|ge\rangle$. Alice and Bob need to perform an EPG operation on four SiV⁻ center systems $\text{Si}_1^1\text{Si}_2^1 - \text{Si}_1^4\text{Si}_2^4$ in the subset using four-dimensional photonic Bell state $|\Psi_{00}\rangle_{CD}$. Then, Alice and Bob measure the spatial-mode states of two photons C and D , and they can read out the amplitude index n' of this EPG operation. The relationship between n' and the position (y_e) of the error SiV⁻ center system can be expressed as

n'	0	1	2	3
y_e	4	1	2	3

The procedure of EPG operation can be simplified for this condition. That is, the hybrid CX gates are performed on photon C (D) and SiV⁻ center Si_1^y (Si_2^y) for y times when $y = 1, 2, 3$, i.e., the four-dimensional photonic Bell state does not interact with $\text{Si}_1^4\text{Si}_2^4$. With this simplified EPG procedure, the four-dimensional photonic Bell state only interacts with three pairs of SiV⁻ centers, and the relationship between n' and y_e is the same as the aforementioned EPG procedure. With the EPG operation, the error SiV⁻ center system $\text{Si}_1^{y_e}\text{Si}_2^{y_e}$ can be read out by the amplitude index n' , and the fidelity of the purified state is $F' = 1$ in this condition.

c. $n = 2$. In this condition, the number of error SiV⁻ center systems in this subset is $n_e = 2$, which corresponds to the configuration that two SiV⁻ center systems in this subset are in state $|ge\rangle$. There are six possible scenarios for the positions of two error SiV⁻ center systems, and the four SiV⁻ center systems in this subset are randomly divided into two groups (named G_1 and G_2), with each group containing two pairs of SiV⁻ center. Then, Alice and Bob perform the ENG operation on group G_1 with a new four-dimensional photonic Bell state $|\Psi_{00}\rangle_{A'B'}$. With the measurement result of photonic Bell state $|\Psi_{00}\rangle_{A'B'}$, three configurations can be obtained with the amplitude index n_1 of the ENG. The relationships of n_1 and three configurations with their probabilities are expressed as

n_1	Configuration	Probability
0	Two error SiV ⁻ center systems in G_2	1/6
2	Two error SiV ⁻ center systems in G_1	1/6
1	One error SiV ⁻ center system in each group	2/3

For $n_1 = 0$ (or $n_1 = 2$), two error SiV⁻ center systems are both in the group G_2 (or G_1), so Alice and Bob can discard the group with two error SiV⁻ center systems and keep the group with no error SiV⁻ center system. For $n_1 = 1$, there is one error SiV⁻ center system in each group, so Alice and Bob have to perform EPG operations on the SiV⁻ center systems of two groups, G_1 and G_2 , with four-dimensional photonic Bell states $|\Psi_{00}\rangle_{CD}$ and $|\Psi_{00}\rangle_{C'D'}$, respectively. In EPG operation, the hybrid CX gates only need to be performed on the SiV⁻ centers in position 1 of each group. After the simplified EPG operation, if the measurement result of photonic Bell state $|\Psi_{00}\rangle_{CD}$ (or $|\Psi_{00}\rangle_{C'D'}$) shows the amplitude index

is $n' = 0$ (or $n'_1 = 0$), it means the error SiV⁻ center system is in the position $y_e = 2$ of group G_1 (or G_2). If the measurement result of photonic Bell state $|\Psi_{00}\rangle_{CD}$ (or $|\Psi_{00}\rangle_{C'D'}$) shows the amplitude index is $n' = 1$ (or $n'_1 = 1$), it means the error SiV⁻ center system is in the position $y_e = 1$ of group G_1 (or G_2).

In order to reduce the resource consumption, the four-dimensional photonic Bell states (i.e., $|\Psi_{00}\rangle_{CD}$ and $|\Psi_{00}\rangle_{C'D'}$) can be replaced by two-dimensional photonic Bell states (e.g., $|\Psi'_{00}\rangle_{IJ}$) in the procedures of EPG operations for two groups. The two-dimensional photonic Bell state is defined as $|\Psi'_{mn}\rangle_{IJ} = \frac{1}{\sqrt{2}} \sum_{k=0}^1 e^{i\pi km} |l_k\rangle_I |t_{k\oplus n}\rangle_J$ ($IJ = CD, C'D'$ and $m, n = 0, 1$), where $|l_k\rangle_I$ and $|t_{k\oplus n}\rangle_J$ represent the spatial modes of photons I and J , respectively. After the hybrid CX gates in EPG operation are performed on the SiV⁻ centers in position 1 of each group, the position of error SiV⁻ center system in each group can also be identified by the measurement results of two-dimensional photonic Bell states. With these ENG and EPG operations, the fidelity of the purified state of this condition is $F' = 1$.

d. $n = 3$. In this condition, the number of error SiV⁻ center systems in this subset is $n_e = 3$, which corresponds to the configuration that three SiV⁻ center systems in this subset are in state $|ge\rangle$. Alice and Bob need to perform EPG operation on four SiV⁻ center systems $\text{Si}_1^1\text{Si}_2^1 - \text{Si}_1^4\text{Si}_2^4$ in the subset using four-dimensional photonic Bell state $|\Psi_{00}\rangle_{CD}$. Then, Alice and Bob measure the spatial-mode states of two photons, C and D , and they can read out the amplitude index n' of this EPG operation. The positions of three error SiV⁻ center systems (y_e^1, y_e^2, y_e^3) satisfy the relationship $n' = (y_e^1 + y_e^2 + y_e^3) \bmod 4$. Here, the relationship between n' and positions of three error SiV⁻ center systems can be expressed as

n'	0	1	2	3
y_e^1, y_e^2, y_e^3	1,3,4	2,3,4	1,2,3	1,2,4

As a result, the positions of error SiV⁻ center systems can be identified by the EPG operation, and the fidelity of the purified state in this condition is $F' = 1$.

In summary, for amplitude damping noise, the number of error SiV⁻ center systems in the subset can be identified by the measurement results of the spatial-mode states of photons A and B in ENG. Subsequently, Alice and Bob have to perform different operations according to the amplitude index n of the ENG operation as shown in Table I. For the conditions $n = 1, 2, 3$, the position of error SiV⁻ center systems in the subset can be identified by ENG and EPG operations, so the purified state is $|\phi^+\rangle$ with fidelity $F' = 1$. For the condition $n = 0$, the purified state is $\rho_2 = \frac{F^4}{F^4+(1-F)^4} |\phi^+\rangle\langle\phi^+| + \frac{(1-F)^4}{F^4+(1-F)^4} |ge\rangle\langle ge|$ with fidelity $F' = \frac{F^4}{F^4+(1-F)^4}$ ($F' > F$ for $F > 1/2$). When $F = 0.8$, the fidelity of mixed state ρ_2 is $F' = 0.996$, which is approximate to $F' = 1$. If the EPG operation is used in the condition $n = 0$, the purified state of SiV⁻ center systems in the subset will be $|\phi^+\rangle$ with fidelity $F' = 1$, but it will cause a resource consumption problem associated with auxiliary entanglement.

TABLE II. The relationship of n, n_e , configuration, additional operations, and fidelity of purified state for the case $p_1 = 0$.

n	n_e	Configuration	Additional operation	F'
0	0 or 4	$4 \times \phi^+\rangle$ or $4 \times eg\rangle$	/	$\frac{F^4}{F^4+(1-F)^4}$
1	3	$3 \times eg\rangle$	EPG	1
2	2	$2 \times eg\rangle$	Grouping	1
3	1	$1 \times eg\rangle$	EPG	1

2. $p_1 = 0$

In this case, the quantum state of the SiV⁻ center system in Eq. (11) can be expressed as

$$\rho_3 = F |\phi^+\rangle\langle\phi^+| + (1-F) |eg\rangle\langle eg|. \quad (15)$$

The detailed procedure of EIEPP for this case is similar to the one for the case $p_2 = 0$ in Sec. III B 1. Alice and Bob perform the ENG operation on four SiV⁻ center systems $\text{Si}_1^1\text{Si}_2^1 - \text{Si}_1^4\text{Si}_2^4$ in a subset using four-dimensional photonic Bell state $|\Psi_{00}\rangle_{AB}$ as the auxiliary, and they measure the spatial-mode states of two photons A and B and read out the number (n_e) of error SiV⁻ center systems (i.e., $|eg\rangle\langle eg|$) in this subset using the relationship $n = (4 - n_e) \bmod 4$. Subsequently, Alice and Bob have to perform different operations for the four conditions obtained by the amplitude index n of this ENG operation. The relationships of n, n_e , configuration, additional operations, and fidelity of purified state are shown in Table II.

For the conditions $n = 2$ (i.e., $n_e = 2$) and $n = 0$ (i.e., $n_e = 0$ or $n_e = 4$), the additional operations are the same as the ones for the case $p_2 = 0$ in Sec. III B 1. For the condition $n = 1$ (i.e., $n_e = 3$), the positions of error SiV⁻ center systems in the subset can be identified by the EPG using the relationship $n' = [4 - (\sum_{y_e=1}^{y_e=n_e} y_e)] \bmod 4$. For the condition $n = 3$ (i.e., $n_e = 1$), Alice and Bob perform the EPG operation on the SiV⁻ center systems in the subset and discard the SiV⁻ center system $\text{Si}_1^{y_e}\text{Si}_2^{y_e}$, where the position of the error SiV⁻ center system is $n' = (4 - y_e) \bmod 4$. After these additional operations, the fidelity of the purified state is $F' = 1$ for the conditions $n = 1, 2, 3$. For the condition $n = 0$, the purified state of the SiV⁻ center system in this subset is mixed state $\rho_4 = \frac{F^4}{F^4+(1-F)^4} |\phi^+\rangle\langle\phi^+| + \frac{(1-F)^4}{F^4+(1-F)^4} |eg\rangle\langle eg|$ with fidelity $F' = \frac{F^4}{F^4+(1-F)^4}$ ($F' > F$ for $F > 1/2$).

3. $p_1 = p_2$

In this case, the quantum state of the SiV⁻ center system in Eq. (11) can be expressed as

$$\rho_5 = F |\phi^+\rangle\langle\phi^+| + \frac{1-F}{2} (|ge\rangle\langle ge| + |eg\rangle\langle eg|), \quad (16)$$

which means the maximally entangled Bell state $|\phi^+\rangle$ could be decayed to the error components $|ge\rangle$ and $|eg\rangle$ with the same probability $\frac{1-F}{2}$. The quantum state in Eq. (16) can be achieved by sending a Bell state through a quantum channel with dephasing noise or bit-flip noise [54,55]. Alice and Bob perform the ENG operation on four SiV⁻ center systems $\text{Si}_1^1\text{Si}_2^1 - \text{Si}_1^4\text{Si}_2^4$ in a subset using four-dimensional photonic Bell state $|\Psi_{00}\rangle_{AB}$ as the auxiliary, and they measure the

TABLE III. The relationship of n , n_e , configuration, probability, and fidelity of purified state for the case $p_1 = p_2$.

n	n_e	Configuration	Probability	F'
0	0	$4 \times \phi^+\rangle$	$F^4 + 8\left(\frac{1-F}{2}\right)^4 + 12F^2\left(\frac{1-F}{2}\right)^2$	$\frac{F^4 + 6F^2\left(\frac{1-F}{2}\right)^2}{F^4 + 8\left(\frac{1-F}{2}\right)^4 + 12F^2\left(\frac{1-F}{2}\right)^2}$
	2	$1 \times ge\rangle + 1 \times eg\rangle$		
	4	$4 \times ge\rangle$ or $4 \times eg\rangle$ or $2 \times ge\rangle + 2 \times eg\rangle$		
1	1	$1 \times ge\rangle$	$4F^3\left(\frac{1-F}{2}\right) + 16F\left(\frac{1-F}{2}\right)^3$	$\frac{F^3\left(\frac{1-F}{2}\right) + \frac{2}{3}F\left(\frac{1-F}{2}\right)^3}{F^3\left(\frac{1-F}{2}\right) + 4F\left(\frac{1-F}{2}\right)^3}$
	3	$3 \times eg\rangle$ or $2 \times ge\rangle + 1 \times eg\rangle$		
2	2	$2 \times ge\rangle$ or $2 \times eg\rangle$	$12F^2\left(\frac{1-F}{2}\right)^2 + 8F\left(\frac{1-F}{2}\right)^4$	1
	4	$3 \times ge\rangle + 1 \times eg\rangle$ or $1 \times ge\rangle + 3 \times eg\rangle$		
3	1	$1 \times eg\rangle$	$4F^3\left(\frac{1-F}{2}\right) + 16F\left(\frac{1-F}{2}\right)^3$	$\frac{F^3\left(\frac{1-F}{2}\right) + \frac{2}{3}F\left(\frac{1-F}{2}\right)^3}{F^3\left(\frac{1-F}{2}\right) + 4F\left(\frac{1-F}{2}\right)^3}$
	3	$3 \times ge\rangle$ or $2 \times eg\rangle + 1 \times ge\rangle$		

spatial-mode states of two photons A and B . As there are two error components in mixed state ρ_5 , it is difficult to directly read out the number of error SiV⁻ center systems in $|ge\rangle$ (or $|eg\rangle$) using the amplitude index n of the four-dimensional photonic Bell state in this ENG. Therefore, Alice and Bob need to perform different operations for the four conditions obtained by the amplitude index n of this ENG. The relationships of n , n_e , configuration, probability, and fidelity of purified state are shown in Table III.

If the amplitude index of ENG is $n = 0$, Alice and Bob will end the protocol without additional operations, and the fidelity of the purified state satisfies $F' > F$ when $F > 0.34$. If the amplitude index of ENG is $n = 1$ (or $n = 3$), Alice and Bob perform the EPG operation on the SiV⁻ center systems in the subset, and they discard the SiV⁻ center system $\text{Si}_1^y \text{Si}_2^y$ in the subset according to the relationship $n' = y \bmod 4$ [or $n' = (4 - y) \bmod 4$] with the amplitude index n' of this EPG, where the fidelity of the purified state satisfies $F' > F$ for $F > 0.5$.

If the amplitude index of ENG is $n = 2$, Alice and Bob equally divide the four SiV⁻ center systems in the subset into two groups. Then, they perform ENG operations on SiV⁻ center systems of the two groups. If the amplitude indexes of the four-dimensional photonic Bell states in the two ENG operations are both $n_1 = 1$ (or $n_1 = 3$), it means there is one error SiV⁻ center system in $|ge\rangle$ (or $|eg\rangle$) in each group, and they can use EPG operations to identify the positions of the error SiV⁻ center systems. If the amplitude index of ENG for a group is $n_1 = 0$, Alice and Bob can discard the SiV⁻ center systems in the other group. They perform EPG operation on the reserved group, and they will reserve this group when $n' = 0$ and discard this group for the other cases. If the amplitude index of ENG for a group is $n_1 = 2$, Alice and Bob can discard the SiV⁻ center systems in this group. They perform the EPG operation on the other reserved group, and they will reserve this group when $n' = 0$ and discard this group for the other cases.

According to the above analysis, if the result of the first ENG operation is $n = 2$, the fidelity of the purified state can achieve $F' = 1$. If $n = 0$, the fidelity of the purified state satisfies $F' > F$ for $F > 0.34$. If $n = 1$ ($n = 3$), the fidelity of the

purified state satisfies $F' > F$ for $F > 0.5$. For $n = 0, 1, 3$, F' can be further increased by dividing the subset into two groups and performing ENG and EPG operations on SiV⁻ center systems in two groups, which is similar to $n = 2$. All the error SiV⁻ center systems in the subset can be fully identified by using enough ENG and EPG operations [54,55]. However, it will cause a resource consumption problem associated with auxiliary entanglement, which makes full identification of all the error components in Eq. (16) challenging.

4. $p_1 \neq p_2 \neq 0$

In this case, the quantum state of the SiV⁻ center system can be expressed as Eq. (11), which corresponds to the condition where the maximally entangled Bell state $|\phi^+\rangle$ could be decayed to the error components $|ge\rangle$ and $|eg\rangle$ with unequal probabilities. The detailed procedure of EIEPP for this case is similar to the one in Sec. III B 3. Alice and Bob perform the ENG operation on four SiV⁻ center systems $\text{Si}_1^y \text{Si}_2^y - \text{Si}_1^y \text{Si}_2^y$ in a subset, and they perform different operations for the four conditions according to the amplitude index n of this ENG. That is, when $n = 0$ and $n = 2$, the additional operations are the same as the ones for the case $p_1 = p_2$ in Sec. III B 3. When $n = 1$ and $n = 3$, Alice and Bob perform the EPG operation on the SiV⁻ center systems in the subset, and they will discard the SiV⁻ center systems on the basis of the amplitude index n' and the comparison of p_1 and p_2 . The relationships of n , the comparison of p_1 and p_2 , n' , and the position y of the discarded SiV⁻ center system in the subset can be expressed as

n	Comparison	$n'(y)$
1	$p_1 > p_2$	$n' = y \bmod 4$
	$p_1 < p_2$	$n' = [4 - (y_1 + y_2 + y_3)] \bmod 4$
3	$p_1 > p_2$	$n' = (y_1 + y_2 + y_3) \bmod 4$
	$p_1 < p_2$	$n' = (4 - y) \bmod 4$

Here, we give two examples (ρ_6 and ρ_7) to illustrate the fidelity of the purified state in this case. The initial mixed state

ρ_6 is expressed as

$$\rho_6 = F|\phi^+\rangle\langle\phi^+| + \frac{2(1-F)}{3}|ge\rangle\langle ge| + \frac{1-F}{3}|eg\rangle\langle eg|, \quad (17)$$

and the fidelity of the purified state after EIEPP can be expressed as

n	F'
0	$\frac{F^4 + 3F^2\left(\frac{1-F}{3}\right)^2 + 3F^2\left[\frac{2}{3}(1-F)\right]^2}{F^4 + \left(\frac{1-F}{3}\right)^2\left\{6F^2 + \left(\frac{1-F}{3}\right)^2\right\} + \left[\frac{2}{3}(1-F)\right]^2\left\{6F^2 + 6\left(\frac{1-F}{3}\right)^2 + \left[\frac{2}{3}(1-F)\right]^2\right\}}$
1	$\frac{F^3\left[\frac{2}{3}(1-F)\right] + \frac{1}{3}F\left(\frac{1-F}{3}\right)^3 + \frac{1}{3}F\left[\frac{2}{3}(1-F)\right]^2\left(\frac{1-F}{3}\right)}{F^3\left[\frac{2}{3}(1-F)\right] + F\left(\frac{1-F}{3}\right)^3 + 3F\left[\frac{2}{3}(1-F)\right]^2\left(\frac{1-F}{3}\right)}$
2	1
3	$\frac{F^3\left(\frac{1-F}{3}\right) + F\left[\frac{2}{3}(1-F)\right]^3 + F\left[\frac{2}{3}(1-F)\right]\left(\frac{1-F}{3}\right)^2}{F^3\left(\frac{1-F}{3}\right) + F\left[\frac{2}{3}(1-F)\right]^3 + 3F\left[\frac{2}{3}(1-F)\right]\left(\frac{1-F}{3}\right)^2}$

If $n = 0$ ($n = 1$), the fidelity of the purified state satisfies $F' > F$ for $F > 0.32$ ($F > 0.41$). If $n = 3$, the fidelity of the purified state satisfies $F' > F$ for $1 > F > 0$.

The mixed state ρ_7 is expressed as

$$\rho_7 = F|\phi^+\rangle\langle\phi^+| + \frac{1-F}{3}|ge\rangle\langle ge| + \frac{2(1-F)}{3}|eg\rangle\langle eg|, \quad (18)$$

and the fidelity of the purified state after EIEPP can be expressed as

n	F'
0	$\frac{F^4 + 3F^2\left(\frac{1-F}{3}\right)^2 + 3F^2\left[\frac{2}{3}(1-F)\right]^2}{F^4 + \left(\frac{1-F}{3}\right)^2\left\{6F^2 + \left(\frac{1-F}{3}\right)^2\right\} + \left[\frac{2}{3}(1-F)\right]^2\left\{6F^2 + 6\left(\frac{1-F}{3}\right)^2 + \left[\frac{2}{3}(1-F)\right]^2\right\}}$
1	$\frac{F^3\left(\frac{1-F}{3}\right) + F\left[\frac{2}{3}(1-F)\right]^3 + F\left[\frac{2}{3}(1-F)\right]\left(\frac{1-F}{3}\right)^2}{F^3\left(\frac{1-F}{3}\right) + F\left[\frac{2}{3}(1-F)\right]^3 + 3F\left[\frac{2}{3}(1-F)\right]\left(\frac{1-F}{3}\right)^2}$
2	1
3	$\frac{F^3\left[\frac{2}{3}(1-F)\right] + \frac{1}{3}F\left(\frac{1-F}{3}\right)^3 + \frac{1}{3}F\left[\frac{2}{3}(1-F)\right]^2\left(\frac{1-F}{3}\right)}{F^3\left[\frac{2}{3}(1-F)\right] + F\left(\frac{1-F}{3}\right)^3 + 3F\left[\frac{2}{3}(1-F)\right]^2\left(\frac{1-F}{3}\right)}$

If $n = 0$ ($n = 3$), the fidelity of the purified state satisfies $F' > F$ for $F > 0.32$ ($F > 0.41$). If $n = 1$, the fidelity of the purified state satisfies $F' > F$ for $1 > F > 0$.

IV. DISCUSSION

In EIEPP, the hybrid CX gate for the SiV⁻ center and the four-dimensional photon state is the basic unit of ENG and EPG. In the ideal condition with strong coupling strength ($g \gg \sqrt{\gamma\kappa}$), the reflection and transmission coefficients of the SiV⁻-WGM-waveguides system are $r \rightarrow 0$ and $t \rightarrow 1$. In experiment, the experimental parameters of imperfect local operations could affect the fidelity and efficiency of the

hybrid CX gate. For example, the fidelity of hybrid CX gates for $p_2 = 0$ (in Sec. III B 1) can be defined as $F_z = |\langle\varphi_0|\varphi_f\rangle|^2$ ($z = ge, 00$), where $|\varphi_0\rangle$ represents the ideal final state and $|\varphi_f\rangle$ represents the experimental final state. F_{ge} (F_{00}) represents the fidelity of hybrid CX gates for $|ge\rangle$ ($|\phi^+\rangle$) and $|\Psi_{0n}\rangle_{AB}$. The efficiency of hybrid CX gates is defined as the probability of a pair of photons (e.g., AB) to be detected after they pass through the SiV⁻-WGM-waveguides systems. In the resonance condition ($\omega_c = \omega_p = \omega_g$), the experimental final state of hybrid CX gates can be obtained as

$$\begin{aligned} |ge\rangle|\Psi_{0n}\rangle_{AB} &\rightarrow |ge\rangle \otimes (t|\Psi_{0n\oplus 1}\rangle_{AB} - r|\Psi_{0n}\rangle_{AB}), \\ |\phi^+\rangle|\Psi_{0n}\rangle_{AB} &\rightarrow \frac{1}{2}[\phi^+|\Psi_{0n}\rangle_{AB}(r^2 + t^2 + 1) \\ &\quad + |\phi^-\rangle|\Psi_{0n}\rangle_{AB}(r^2 + t^2 - 1) \\ &\quad - rt|\phi^+\rangle|\Psi_{0n\oplus 1}\rangle_{AB} - rt|\phi^+\rangle|\Psi_{0n\oplus 3}\rangle_{AB} \\ &\quad - rt|\phi^-\rangle|\Psi_{0n\oplus 1}\rangle_{AB} - rt|\phi^-\rangle|\Psi_{0n\oplus 3}\rangle_{AB}], \end{aligned} \quad (19)$$

where t and r represent transmission and reflection coefficients in Eq. (4). Hence, the fidelity and efficiency of hybrid CX gates can be expressed as

$$\begin{aligned} F_{ge} &= \frac{t^2}{r^2 + t^2}, \\ F_{00} &= \frac{(r^2 + t^2 + 1)^2}{(r^2 + t^2 + 1)^2 + (r^2 + t^2 - 1)^2 + 4r^2t^2}, \\ E_{ge} &= r^2 + t^2, \\ E_{00} &= (r^2 + t^2 + 1)^2 + (r^2 + t^2 - 1)^2 + 4r^2t^2, \end{aligned} \quad (20)$$

where E_{ge} (E_{00}) represents the efficiency of hybrid CX gates for $|ge\rangle$ ($|\phi^+\rangle$) and $|\Psi_{0n}\rangle_{AB}$. The fidelity and efficiency of hybrid CX gates as the function of $g/(\kappa\gamma)^{1/2}$ are shown in Fig. 5. The dips in Figs. 5(a) and 5(b) show the minimum values of fidelity and efficiency with $-r = t$. In the strong coupling regime with $g \gg (\kappa\gamma)^{1/2}$ and $-r \ll t$, the fidelity and efficiency of hybrid CX gates are high, which are close to the ideal condition. For example, when $g/(\kappa\gamma)^{1/2} > 4.1$ [59], the fidelities of hybrid CX gates are $F_{ge} > 99.999\%$ and $F_{00} > 99.998\%$, and the efficiencies are $E_{ge} > 99.384\%$ and $E_{00} > 99.387\%$ when $g/(\kappa\gamma)^{1/2} > 12.7$. In the weak coupling regime with $-r > t$, the fidelity and efficiency of the hybrid CX gates for $|\phi^+\rangle$ and $|\Psi_{0n}\rangle_{AB}$ are also increased compared with the values in the dips, as the wrong output ports of photons will also achieve the correct output quantum state in certain cases. In addition, in the SiV⁻-WGM-waveguides system, the decoherence of the SiV⁻ center could also decrease the fidelity of the hybrid CX gate with $[1 + e^{-t\tau/T_e}]/2$ [73,74]. However, the scattering time $t\tau$ is in the microsecond range, and the electron spin coherence time T_e exceeds 10 ms at 100 mK [75], which will cause little influence in the fidelity of the hybrid CX gate.

The experimental influence of the hybrid CX gate will affect the fidelity of the purified state of the SiV⁻ center system in EIEPP. The average fidelity of the purified state in the ideal condition can be defined by $\langle F' \rangle_4^{\text{ideal}} = \sum_{n=0}^{n=3} P(n)F'(n)$. $F'(n)$ stands for the fidelity F' when the amplitude index of the first ENG is n . $P(n)$

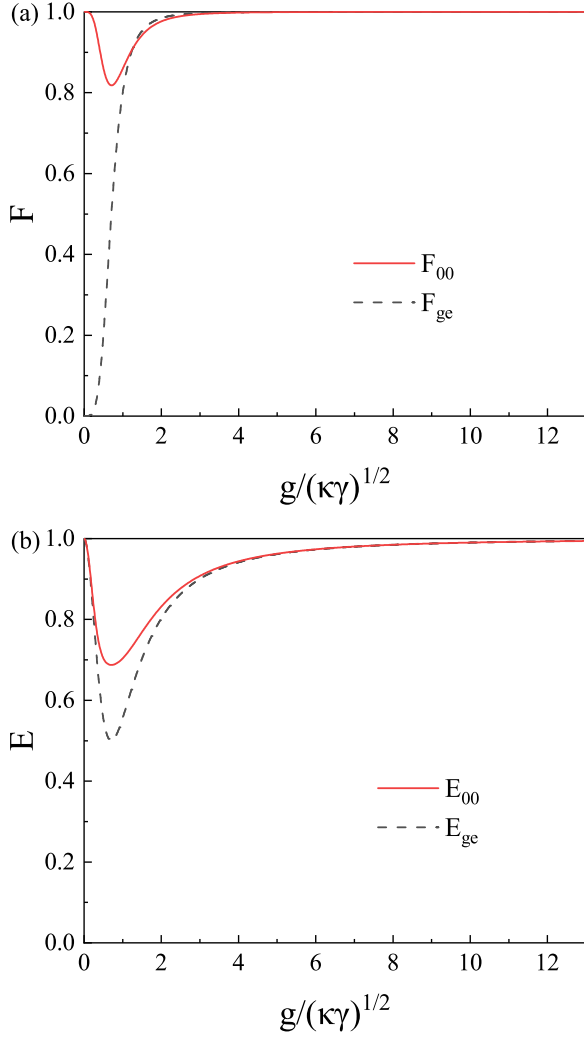


FIG. 5. The (a) fidelity and (b) efficiency of the hybrid CX gates for $|ge\rangle$ ($|\phi^+\rangle$) and $|\Psi_{0n}\rangle_{AB}$ as the function of the parameter $g/(\kappa\gamma)^{1/2}$.

represents the probability of obtaining the amplitude index n in the first ENG, where $P(n) = C_4^n F^{4-n} (1-F)^n$ for $n = 1, 2, 3$ and $P(0) = F^4 + (1-F)^4$. In practical application, the nonunit fidelity of the hybrid CX gate will affect the average fidelity of the purified state in EIEPP. For $p_2 = 0$ in Sec. III B 1, the average fidelity of the purified state in the experimental condition can be expressed as

$$\begin{aligned} \langle F' \rangle_4 &= F^4 F_{00}^4 + F^3 (1-F) \sum_{w=6}^9 F_{00}^w F_{ge}^{10-w} \\ &\quad + 6F^2 (1-F)^2 F_{00}^2 F_{ge}^2 \\ &\quad + 4F (1-F)^3 F_{00} F_{ge}^3, \end{aligned} \quad (21)$$

where the EIEPP is terminated at $n \geq 2$ to reduce the resource consumption. In Fig. 6(a), the fidelity $\langle F' \rangle_4$ is calculated as the function of $g/(\kappa\gamma)^{1/2}$ for $F = 0.9$. It is obvious that $\langle F' \rangle_4$ is greater in the strong coupling regime. For example, when $F = 0.9$ ($F = 0.8$) and $g/(\kappa\gamma)^{1/2} > 4.1$ [59], $\langle F' \rangle_4 > 99.1\%$ ($\langle F' \rangle_4 > 98.9\%$).

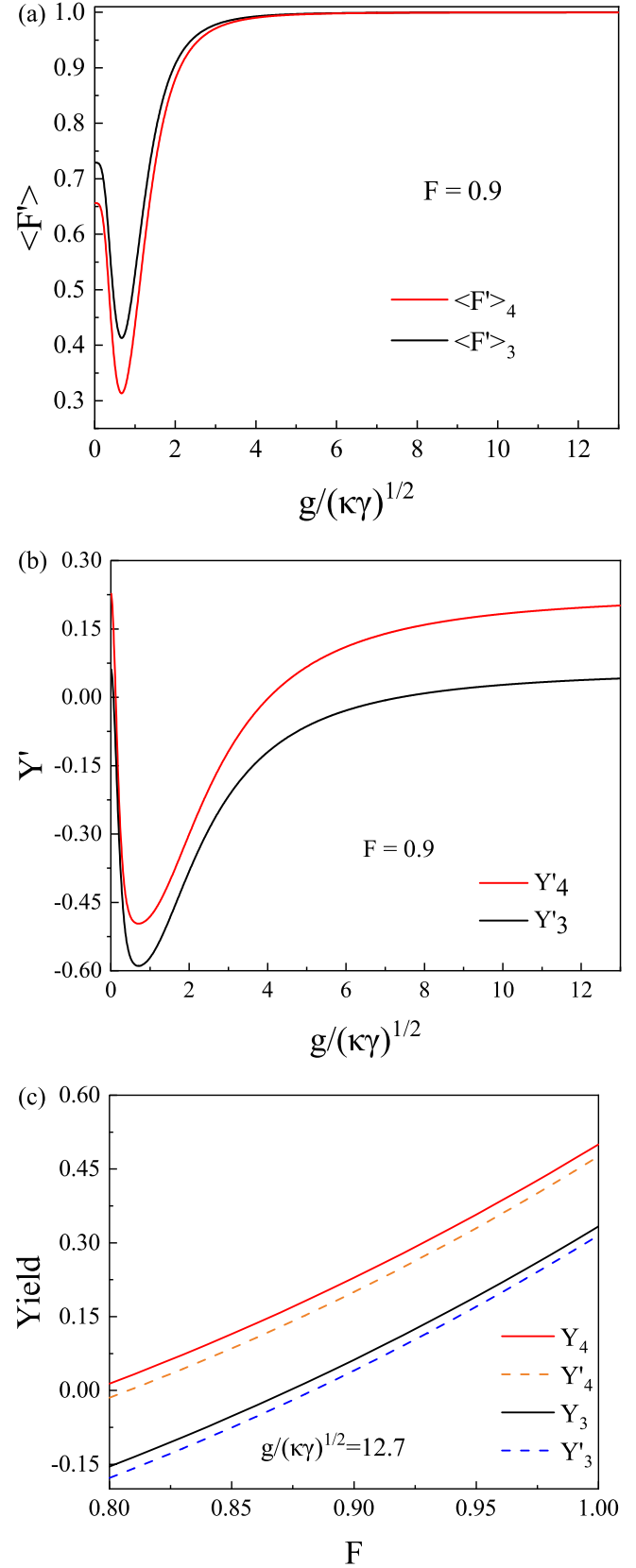


FIG. 6. (a) Average fidelity $\langle F' \rangle$ and (b) yield Y' as the function of the parameter $g/(\kappa\gamma)^{1/2}$ with initial fidelity $F = 0.9$. (c) Yields under ideal and experimental conditions as the function of initial fidelity F , where the experimental parameters satisfy $g/(\kappa\gamma)^{1/2} = 12.7$.

Another important metric for the entanglement purification protocol is yield. In the ideal condition, the yield of EIEPP in Sec. III is defined as [54,55]

$$Y = \frac{-2 + \sum_{n=0}^3 P(n)[4 - n - R(n)]}{4}, \quad (22)$$

where the consumed auxiliary entanglement is also taken into account. Here, -2 represents the four-dimensional photonic Bell state with 2 ebits, while 4 represents four SiV⁻ center Bell states in a subset with 4 ebits. $R(n)$ is the auxiliary entanglement resource needed to identify the positions of error SiV⁻ center systems. For different amplitude index n of the first ENG, $R(n)$ will be different. For example, for the case $p_2 = 0$ in Sec. III B 1, the relationship of n and $R(n)$ can be expressed as

n	0	1	2	3
$R(n)$	0	2	10/3	2.

The yield of EIEPP for $p_2 = 0$ in Sec. III B 1 can be expressed as

$$Y_4 = [4F^4 + 4(1 - F)^4 + 12F^3(1 - F) - 2 - 8F^3(1 - F)]/4, \quad (23)$$

where the EIEPP is terminated at $n \geq 2$ in the ideal condition. Due to experimental influence, the efficiency of the hybrid CX gates will affect the yield of EIEPP, and the yield of EIEPP (terminated at $n \geq 2$) for $p_2 = 0$ can be expressed as

$$Y'_4 = \left[4F^4 E_{00}^4 + 4(1 - F)^4 E_{ge}^4 + 3F^3(1 - F) \sum_{w=6}^9 E_{00}^w E_{ge}^{10-w} - 2 - 8F^3(1 - F) \right] / 4. \quad (24)$$

In Fig. 6(b), the yield Y'_4 of EIEPP is calculated as the function of $g/(\kappa\gamma)^{1/2}$ for $F = 0.9$. In Fig. 6(c), the yield Y_4 of EIEPP is calculated as the function of initial fidelity F . It can be found that the yield of EIEPP is greater in the strong coupling regime. For example, when $F > 0.9$, $Y_4 > 22.91\%$ is achieved in the ideal condition. Considering the experimental influence, when $g/(\kappa\gamma)^{1/2} > 12.7$, $Y'_4 > 20\%$ is achieved for $F > 0.9$.

In the EIEPP introduced in Sec. III, the nonlocal mixed entangled SiV⁻ center systems are divided into several subsets, and each subset contains four nonlocal mixed entangled SiV⁻ center systems. The number (L) of nonlocal mixed entangled SiV⁻ center systems in a subset can be adjusted, and the yield of EIEPP will be increased with the increase of L . For example, for $p_2 = 0$ in Sec. III B 1, if $L = 1$, the yield of EIEPP is $Y_1 = F - 2$ in the ideal condition, which is a negative value. The negative yield signifies that the entanglement resource gained in EIEPP is less than the one consumed. If $L = 3$, the yield of EIEPP in the ideal condition can be expressed

as [54,55]

$$Y_3 = \frac{3F^3 + 6F^2(1 - F) - 2 - 6F^2(1 - F)}{3}, \quad (25)$$

where the EIEPP is terminated at $n \geq 2$. The yield of EIEPP (terminated at $n \geq 2$) in the experimental condition can be expressed as

$$Y'_3 = \left[3F^3 E_{00}^3 + 2F^2(1 - F) \sum_{w'=5}^7 E_{00}^{w'} E_{ge}^{9-w'} - 2 - 6F^2(1 - F) \right] / 3. \quad (26)$$

In Fig. 6(c), the yields Y_3 and Y'_3 of EIEPP are calculated as the function of F , where the experimental parameters satisfy $g/(\kappa\gamma)^{1/2} = 12.7$. From Fig. 6(c), it is obvious that Y_3 and Y'_3 have positive values, and Y_4 (Y'_4) is larger than Y_3 (Y'_3).

If the number of nonlocal mixed entangled SiV⁻ center systems in a subset is increased from $L = 3$ to $L = 4$, the fidelity of the purified state will be decreased. For $p_2 = 0$ in Sec. III B 1, if $L = 3$, the purified state will have unit fidelity in the ideal condition, and the average fidelity of the purified state in the experimental condition can be expressed as

$$\langle F' \rangle_3 = F^3 F_{00}^3 + F^2(1 - F) \sum_{w'=5}^7 F_{00}^{w'} F_{ge}^{9-w'} + 3F(1 - F)^2 F_{00} F_{ge}^2 + (1 - F)^3 F_{ge}^3, \quad (27)$$

where the EIEPP is terminated at $n \geq 2$. In Fig. 6(a), the fidelity $\langle F' \rangle_3$ is calculated as the function of $g/(\kappa\gamma)^{1/2}$ for $F = 0.9$. When $F = 0.9$ ($F = 0.8$) and $g/(\kappa\gamma)^{1/2} > 4.1$, $\langle F' \rangle_3 > 99.3\%$ ($\langle F' \rangle_3 > 99.2\%$). It is obvious that $\langle F' \rangle_3$ is a little higher than $\langle F' \rangle_4$, and the difference between these two average fidelities will be un conspicuous with the increase of coupling strength. However, the yield of EIEPP will be largely increased when the number L is increased from $L = 3$ to $L = 4$ as shown in Figs. 6(b) and 6(c).

According to the analysis, we can see that the EIEPP has high fidelity and high yield in the strong coupling regime of the SiV⁻-WGM-waveguides-HWP system in Fig. 1(c), while the ultrastrong coupling strength of cavity QED is still a challenge in experiment. Fortunately, several researches have discussed the possibility of achieving high-fidelity quantum operations under the weak coupling regime of cavity QED [48,76–79], which provide an interesting insight to improve the performance of this EIEPP in the weak coupling regime of the SiV⁻-WGM-waveguides-HWP system. Moreover, this EIEPP can also be used to improve the entanglement of other types of quantum stationary systems with similar energy-level structure in Fig. 1(b), such as quantum dot [48], nitrogen vacancy center in diamond [80], and so on.

V. CONCLUSION

In summary, we have introduced an EIEPP for entangled SiV⁻ center systems suffering from several particular types of noise. First, we construct the hybrid CX gate for the SiV⁻ center system and the four-dimensional photon system,

which is the basic unit of ENG and EPG. Then, we construct the ENG and EPG and adopt them to identify the number and position of error SiV^- center systems in an ensemble, resulting in high-fidelity entangled states of SiV^- center systems. This EIEPP has superior performance for SiV^- center systems with amplitude damping noise, and it is also applicable for SiV^- center systems suffering from other types of noise. At last, the fidelity of the purified state and the yield of EIEPP are calculated with experimental parameters of imperfect local operations. If the SiV^- center systems suffer from other noises (e.g., phase-flip noise), the EIEPP is also applicable as any mixed quantum state can be transformed to the distillable state of EIEPP by suitable maps (e.g., depolarization map) and quantum Fourier transformations

[55]. In a word, this EIEPP demonstrates the feasibility of maintaining high-fidelity entanglement of a stationary system with high-dimensional entanglement, thus it has expanded the application prospects of a stationary system and high-dimensional entanglement in quantum information protocols and technologies.

ACKNOWLEDGMENTS

This work was supported by the National Natural Science Foundation of China under Grants No. 11604226, No. 12104251, and No. 11804236, and the Beijing Municipal Commission of Education under Grants No. CIT&TCD201904080 and No. KM201810028005.

-
- [1] H. J. Kimble, The quantum internet, *Nature (London)* **453**, 1023 (2008).
 - [2] S. Wehner, D. Elkouss, and R. Hanson, Quantum internet: A vision for the road ahead, *Science* **362**, eaam9288 (2018).
 - [3] C. H. Bennett and S. J. Wiesner, Communication via one- and two-particle operators on Einstein-Podolsky-Rosen states, *Phys. Rev. Lett.* **69**, 2881 (1992).
 - [4] X.-S. Liu, G.-L. Long, D.-M. Tong, and F. Li, General scheme for superdense coding between multiparties, *Phys. Rev. A* **65**, 022304 (2002).
 - [5] C. H. Bennett, G. Brassard, C. Crépeau, R. Jozsa, A. Peres, and W. K. Wootters, Teleporting an unknown quantum state via dual classical and Einstein-Podolsky-Rosen channels, *Phys. Rev. Lett.* **70**, 1895 (1993).
 - [6] D. Bouwmeester, J.-W. Pan, K. Mattle, M. Eibl, H. Weinfurter, and A. Zeilinger, Experimental quantum teleportation, *Nature (London)* **390**, 575 (1997).
 - [7] M. Hillery, V. Bužek, and A. Berthiaume, Quantum secret sharing, *Phys. Rev. A* **59**, 1829 (1999).
 - [8] Y.-G. Yang, Y.-C. Wang, Y.-L. Yang, X.-B. Chen, D. Li, Y.-H. Zhou, and W.-M. Shi, Participant attack on the deterministic measurement-device-independent quantum secret sharing protocol, *Sci. China Phys. Mech. Astron.* **64**, 260321 (2021).
 - [9] A. K. Ekert, Quantum cryptography based on Bell's theorem, *Phys. Rev. Lett.* **67**, 661 (1991).
 - [10] M. Curty, M. Lewenstein, and N. Lütkenhaus, Entanglement as a precondition for secure quantum key distribution, *Phys. Rev. Lett.* **92**, 217903 (2004).
 - [11] F. Xu, X. Ma, Q. Zhang, H.-K. Lo, and J.-W. Pan, Secure quantum key distribution with realistic devices, *Rev. Mod. Phys.* **92**, 025002 (2020).
 - [12] G.-L. Long and X.-S. Liu, Theoretically efficient high-capacity quantum-key-distribution scheme, *Phys. Rev. A* **65**, 032302 (2002).
 - [13] F.-G. Deng, G.-L. Long, and X.-S. Liu, Two-step quantum direct communication protocol using the Einstein-Podolsky-Rosen pair block, *Phys. Rev. A* **68**, 042317 (2003).
 - [14] W. Zhang, D.-S. Ding, Y.-B. Sheng, L. Zhou, B.-S. Shi, and G.-C. Guo, Quantum secure direct communication with quantum memory, *Phys. Rev. Lett.* **118**, 220501 (2017).
 - [15] L. Zhou and Y.-B. Sheng, One-step device-independent quantum secure direct communication, *Sci. China Phys. Mech. Astron.* **65**, 250311 (2022).
 - [16] H.-J. Briegel, W. Dür, J. I. Cirac, and P. Zoller, Quantum repeaters: The role of imperfect local operations in quantum communication, *Phys. Rev. Lett.* **81**, 5932 (1998).
 - [17] L.-M. Duan, M. D. Lukin, J. I. Cirac, and P. Zoller, Long-distance quantum communication with atomic ensembles and linear optics, *Nature (London)* **414**, 413 (2001).
 - [18] N. Sangouard, C. Simon, H. de Riedmatten, and N. Gisin, Quantum repeaters based on atomic ensembles and linear optics, *Rev. Mod. Phys.* **83**, 33 (2011).
 - [19] M. Zwerger, A. Pirker, V. Dunjko, H. J. Briegel, and W. Dür, Long-range big quantum-data transmission, *Phys. Rev. Lett.* **120**, 030503 (2018).
 - [20] T. Li, G.-J. Yang, and F.-G. Deng, Heralded quantum repeater for a quantum communication network based on quantum dots embedded in optical microcavities, *Phys. Rev. A* **93**, 012302 (2016).
 - [21] W. Dür and H.-J. Briegel, Entanglement purification for quantum computation, *Phys. Rev. Lett.* **90**, 067901 (2003).
 - [22] Y. Li and S. C. Benjamin, High threshold distributed quantum computing with three-qubit nodes, *New J. Phys.* **14**, 093008 (2012).
 - [23] C. H. Bennett, G. Brassard, S. Popescu, B. Schumacher, J. A. Smolin, and W. K. Wootters, Purification of noisy entanglement and faithful teleportation via noisy channels, *Phys. Rev. Lett.* **76**, 722 (1996).
 - [24] C. H. Bennett, D. P. DiVincenzo, J. A. Smolin, and W. K. Wootters, Mixed-state entanglement and quantum error correction, *Phys. Rev. A* **54**, 3824 (1996).
 - [25] W. Dür and H. J. Briegel, Entanglement purification and quantum error correction, *Rep. Prog. Phys.* **70**, 1381 (2007).
 - [26] D. Deutsch, A. Ekert, R. Jozsa, C. Macchiavello, S. Popescu, and A. Sanpera, Quantum privacy amplification and the security of quantum cryptography over noisy channels, *Phys. Rev. Lett.* **77**, 2818 (1996).
 - [27] J. Dehaene, M. Van den Nest, B. De Moor, and F. Verstraete, Local permutations of products of Bell states and entanglement distillation, *Phys. Rev. A* **67**, 022310 (2003).

- [28] Karl Gerd H. Vollbrecht and F. Verstraete, Interpolation of recurrence and hashing entanglement distillation protocols, *Phys. Rev. A* **71**, 062325 (2005).
- [29] H. Bombin and M. A. Martin-Delgado, Entanglement distillation protocols and number theory, *Phys. Rev. A* **72**, 032313 (2005).
- [30] R. Reichle, D. Leibfried, E. Knill, J. Britton, R. B. Blakestad, J. D. Jost, C. Langer, R. Ozeri, S. Seidelin, and D. J. Wineland, Experimental purification of two-atom entanglement, *Nature (London)* **443**, 838 (2006).
- [31] J.-W. Pan, S. Gasparoni, R. Ursin, G. Weihs, and A. Zeilinger, Experimental entanglement purification of arbitrary unknown states, *Nature (London)* **423**, 417 (2003).
- [32] Y.-B. Sheng, F.-G. Deng, and H.-Y. Zhou, Efficient polarization-entanglement purification based on parametric down-conversion sources with cross-Kerr nonlinearity, *Phys. Rev. A* **77**, 042308 (2008).
- [33] K. Fujii and K. Yamamoto, Entanglement purification with double selection, *Phys. Rev. A* **80**, 042308 (2009).
- [34] Y.-B. Sheng and F.-G. Deng, Deterministic entanglement purification and complete nonlocal Bell-state analysis with hyperentanglement, *Phys. Rev. A* **81**, 032307 (2010).
- [35] Y.-B. Sheng and F.-G. Deng, One-step deterministic polarization-entanglement purification using spatial entanglement, *Phys. Rev. A* **82**, 044305 (2010).
- [36] M. Zwerger, H. J. Briegel, and W. Dür, Universal and optimal error thresholds for measurement-based entanglement purification, *Phys. Rev. Lett.* **110**, 260503 (2013).
- [37] B.-C. Ren, F.-F. Du, and F.-G. Deng, Two-step hyperentanglement purification with the quantum-state-joining method, *Phys. Rev. A* **90**, 052309 (2014).
- [38] T.-J. Wang, L.-L. Liu, R. Zhang, C. Cao, and C. Wang, One-step hyperentanglement purification and hyperdistillation with linear optics, *Opt. Express* **23**, 9284 (2015).
- [39] N. Kalb, A. A. Reiserer, P. C. Humphreys, J. J. W. Bakermans, S. J. Kamerling, N. H. Nickerson, S. C. Benjamin, D. J. Twitchen, M. Markham, and R. Hanson, Entanglement distillation between solid-state quantum network nodes, *Science* **356**, 928 (2017).
- [40] L.-K. Chen, H.-L. Yong, P. Xu, X.-C. Yao, T. Xiang, Z.-D. Li, C. Liu, H. Lu, N.-L. Liu, L. Li, T. Yang, C.-Z. Peng, B. Zhao, Y.-A. Chen, and J.-W. Pan, Experimental nested purification for a linear optical quantum repeater, *Nat. Photonics* **11**, 695 (2017).
- [41] T.-J. Wang, S.-C. Mi, and C. Wang, Hyperentanglement purification using imperfect spatial entanglement, *Opt. Express* **25**, 2969 (2017).
- [42] J. Miguel-Ramiro and W. Dür, Efficient entanglement purification protocols for d-level systems, *Phys. Rev. A* **98**, 042309 (2018).
- [43] L. Ruan, W. Dai, and M. Z. Win, Adaptive recurrence quantum entanglement distillation for two-Kraus-operator channels, *Phys. Rev. A* **97**, 052332 (2018).
- [44] F. Rozpedek, T. Schiet, L. P. Thinh, D. Elkouss, A. C. Doherty, and S. Wehner, Optimizing practical entanglement distillation, *Phys. Rev. A* **97**, 062333 (2018).
- [45] K. Fang, X. Wang, M. Tomamichel, and R. Duan, Non-asymptotic entanglement distillation, *IEEE Trans. Inf. Theory* **65**, 6454 (2019).
- [46] K. Fang and Z.-W. Liu, No-go theorems for quantum resource purification, *Phys. Rev. Lett.* **125**, 060405 (2020).
- [47] L. Zhou, W. Zhong, and Y.-B. Sheng, Purification of the residual entanglement, *Opt. Express* **28**, 2291 (2020).
- [48] G.-Y. Wang, Q. Ai, F.-G. Deng, and B.-C. Ren, Imperfect-interaction-free entanglement purification on stationary systems for solid quantum repeaters, *Opt. Express* **28**, 18693 (2020).
- [49] X.-M. Hu, C.-X. Huang, Y.-B. Sheng, L. Zhou, B.-H. Liu, Y. Guo, C. Zhang, W.-B. Xing, Y.-F. Huang, C.-F. Li, and G.-C. Guo, Long-distance entanglement purification for quantum communication, *Phys. Rev. Lett.* **126**, 010503 (2021).
- [50] S. Ecker, P. Sohr, L. Bulla, M. Huber, M. Bohmann, and R. Ursin, Experimental single-copy entanglement distillation, *Phys. Rev. Lett.* **127**, 040506 (2021).
- [51] C.-X. Huang, X.-M. Hu, B.-H. Liu, L. Zhou, Y.-B. Sheng, C.-F. Li, and G.-C. Guo, Experimental one-step deterministic polarization entanglement purification, *Sci. Bull.* **67**, 593 (2022).
- [52] P.-S. Yan, L. Zhou, W. Zhong, and Y.-B. Sheng, Measurement-based logical qubit entanglement purification, *Phys. Rev. A* **105**, 062418 (2022).
- [53] P. Wang, Z. Zhang, C.-Q. Yu, R.-Y. Yuan, F.-F. Du, and B.-C. Ren, Measurement-based hyperentanglement distillation for lossy and distortion photon state, *Ann. Phys. (Berlin)* **535**, 2200505 (2023).
- [54] F. Riera-Sàbat, P. Sekatski, A. Pirker, and W. Dür, Entanglement-assisted entanglement purification, *Phys. Rev. Lett.* **127**, 040502 (2021).
- [55] F. Riera-Sàbat, P. Sekatski, A. Pirker, and W. Dür, Entanglement purification by counting and locating errors with entangling measurements, *Phys. Rev. A* **104**, 012419 (2021).
- [56] H. Zhou, T. Li, and K.-Y. Xia, Parallel and heralded multiqubit entanglement generation for quantum networks, *Phys. Rev. A* **107**, 022428 (2023).
- [57] M. Ruf, N. H. Wan, H. Choi, D. Englund, and R. Hanson, Quantum networks based on color centers in diamond, *J. Appl. Phys.* **130**, 070901 (2021).
- [58] C. T. Nguyen, D. D. Sukachev, M. K. Bhaskar, B. Machielse, D. S. Levonian, E. N. Knall, P. Stroganov, C. Chia, M. J. Burek, R. Riedinger, H. Park, M. Lončar, and M. D. Lukin, An integrated nanophotonic quantum register based on silicon-vacancy spins in diamond, *Phys. Rev. B* **100**, 165428 (2019).
- [59] M. K. Bhaskar, R. Riedinger, B. Machielse, D. S. Levonian, C. T. Nguyen, E. N. Knall, H. Park, D. Englund, M. Lončar, D. D. Sukachev, and M. D. Lukin, Experimental demonstration of memory-enhanced quantum communication, *Nature (London)* **580**, 60 (2020).
- [60] E. Neu, D. Steinmetz, J. Riedrich-Möller, S. Gsell, M. Fischer, M. Schreck, and C. Becher, Single photon emission from silicon-vacancy colour centres in chemical vapour deposition nano-diamonds on iridium, *New J. Phys.* **13**, 025012 (2011).
- [61] L. J. Rogers, K. D. Jahnke, T. Teraji, L. Marseglia, C. Müller, B. Naydenov, H. Schauffert, C. Kranz, J. Isoya, L. P. McGuinness, and F. Jelezko, Multiple intrinsically identical single-photon emitters in the solid state, *Nat. Commun.* **5**, 4739 (2014).
- [62] H. Sternschulte, K. Thonke, R. Sauer, P. C. Münzinger, and P. Michler, 1.681-eV luminescence center in chemical-vapor-deposited homoepitaxial diamond films, *Phys. Rev. B* **50**, 14554 (1994).

- [63] R. E. Evans, A. Sipahigil, D. D. Sukachev, A. S. Zibrov, and M. D. Lukin, Narrow-linewidth homogeneous optical emitters in diamond nanostructures via silicon ion implantation, *Phys. Rev. Appl.* **5**, 044010 (2016).
- [64] B. Hensen, H. Bernien, A. E. Dréau, A. Reiserer, N. Kalb, M. S. Blok, J. Ruitenber, R. F. Vermeulen, R. N. Schouten, C. Abellán, W. Amaya, V. Pruneri, M. W. Mitchell, M. Markham, D. J. Twitchen, D. Elkouss, S. Wehner, T. H. Taminiau, and R. Hanson, Loophole-free Bell inequality violation using electron spins separated by 1.3 kilometres, *Nature (London)* **526**, 682 (2015).
- [65] F. Monifi, S. K. Özdemir, and L. Yang, Tunable add-drop filter using an active whispering gallery mode microcavity, *Appl. Phys. Lett.* **103**, 181103 (2013).
- [66] Y. Louyer, D. Meschede, and A. Rauschenbeutel, Tunable whispering-gallery-mode resonators for cavity quantum electrodynamics, *Phys. Rev. A* **72**, 031801(R) (2005).
- [67] S. M. Spillane, T. J. Kippenberg, K. J. Vahala, K. W. Goh, E. Wilcut, and H. J. Kimble, Ultrahigh-Q toroidal microresonators for cavity quantum electrodynamics, *Phys. Rev. A* **71**, 013817 (2005).
- [68] L.-Y. He, T.-J. Wang, and C. Wang, Construction of high-dimensional universal quantum logic gates using a Λ system coupled with a whispering-gallery-mode microresonator, *Opt. Express* **24**, 15429 (2016).
- [69] D. O’Shea, C. Junge, J. Volz, and A. Rauschenbeutel, Fiber-optical switch controlled by a single atom, *Phys. Rev. Lett.* **111**, 193601 (2013).
- [70] Q. Chen, W.-L. Yang, M. Feng, and J.-F. Du, Entangling separate nitrogen-vacancy centers in a scalable fashion via coupling to microtoroidal resonators, *Phys. Rev. A* **83**, 054305 (2011).
- [71] A. Michael, M. T. Quintino, P. Walther and L. A. Rozema, Higher-order process matrix tomography of a passively-stable quantum switch, *PRX Quantum* **5**, 010325 (2024).
- [72] M. A. Nielsen and I. L. Chuang, *Quantum Computation and Quantum Information* (Cambridge University Press, Cambridge, 2010).
- [73] W. Dür and H.-J. Briegel, Stability of macroscopic entanglement under decoherence, *Phys. Rev. Lett.* **92**, 180403 (2004).
- [74] L. Aolita, D. Cavalcanti, A. Acín, A. Salles, M. Tiersch, A. Buchleitner, and F. de Melo, Scalability of Greenberger-Horne-Zeilinger and random-state entanglement in the presence of decoherence, *Phys. Rev. A* **79**, 032322 (2009).
- [75] D. D. Sukachev, A. Sipahigil, C. T. Nguyen, M. K. Bhaskar, R. E. Evans, F. Jelezko, and M. D. Lukin, Silicon-vacancy spin qubit in diamond: A quantum memory exceeding 10 ms with single-shot state readout, *Phys. Rev. Lett.* **119**, 223602 (2017).
- [76] A. B. Young, C. Y. Hu, and J. G. Rarity, Generating entanglement with low-Q-factor microcavities, *Phys. Rev. A* **87**, 012332 (2013).
- [77] T. Li and F.-G. Deng, Error-rejecting quantum computing with solid-state spins assisted by low-Q optical microcavities, *Phys. Rev. A* **94**, 062310 (2016).
- [78] B.-C. Ren and F.-G. Deng, Robust hyperparallel photonic quantum entangling gate with cavity QED, *Opt. Express* **25**, 10863 (2017).
- [79] G.-Y. Wang, Q. Ai, B.-C. Ren, T. Li, and F.-G. Deng, Error-detected generation and complete analysis of hyperentangled Bell states for photons assisted by quantum-dot spins in double-sided optical microcavities, *Opt. Express* **24**, 28444 (2016).
- [80] E. Togan, Y. Chu, A. S. Trifonov, L. Jiang, J. Maze, L. Childress, M. V. G. Dutt, A. S. Sørensen, P. R. Hemmer, A. S. Zibrov, and M. D. Lukin, Quantum entanglement between an optical photon and a solid-state spin qubit, *Nature (London)* **466**, 730 (2010).